Late Holocene Climate Changes in the Altai Region Based on a First High-Resolution Biomarker Isotope Record From Lake Khar Nuur

Journal Article

Author(s):
Bliedtner, Marcel; Struck, Julian; Strobel, Paul; Salazar, Gary; Szidat, Sönke; Bazarradnaa, Enkhtuya; Lloren, Ronald; Dubois, Nathalie; Zech, Roland

Geophysical Research Letters®

Key Points:

- A high-resolution 4.2 ka paleoclimate record from Lake Khar Nuur in the Mongolian Altai, based on biomarker compound-specific δ^2H analyses
- Our hydrological proxies record distinct changes in warm/wet and cold/dry conditions during the Late Holocene in the Altai Region
- Pronounced warm/wet conditions from ~3.5 to 2.8 cal. ka BP probably favored the widespread dispersal of nomadic pastoralism in the region

Supporting Information:

Supporting Information may be found in the online version of this article.

Correspondence to:

M. Bliedtner,
marcel.bliedtner@uni-jena.de

Author Contributions:

Conceptualization: Marcel Bliedtner, Julian Struck, Paul Strobel, Roland Zech
Formal analysis: Marcel Bliedtner
Investigation: Marcel Bliedtner, Julian Struck, Paul Strobel, Gary Salazar, Ronald Lloren
Writing – original draft: Marcel Bliedtner
Writing – review & editing: Marcel Bliedtner, Julian Struck, Paul Strobel, Gary Salazar, Sönke Szidat, Enkhtuya Bazarradnaa, Ronald Lloren, Nathalie Dubois, Roland Zech

Late Holocene Climate Changes in the Altai Region Based on a First High-Resolution Biomarker Isotope Record From Lake Khar Nuur

Marcel Bliedtner[1] , **Julian Struck[1]** , **Paul Strobel[1]** , **Gary Salazar[2]** , **Sönke Szidat[2]** , **Enkhtuya Bazarradnaa[3]**, **Ronald Lloren[4,5]**, **Nathalie Dubois[4,5]** , and **Roland Zech[1]**

[1]Institute of Geography, Friedrich Schiller University Jena, Jena, Germany, [2]Department of Chemistry, Biochemistry and Pharmaceutical Sciences and Oeschger Centre for Climate Change Research, University of Bern, Bern, Switzerland, [3]Institute of Plant and Agricultural Sciences, Mongolian University of Life Sciences, Darkhan, Mongolia, [4]Department of Surface Waters Research and Management, Eawag, Dübendorf, Switzerland, [5]Department of Earth Sciences, ETH Zürich, Zürich, Switzerland

Abstract The Late Holocene marks a substantial cultural and economic transition in the eastern Eurasian Steppe and Altai Region with the dispersal of nomadic pastoralism. So far, paleoclimate conditions during this time remain unclear and controversial. Here, we present a high-resolution 4.2 ka paleoclimate record from Lake Khar Nuur in the Mongolian Altai that is based on lake sediment proxies and biomarker compound-specific δ^2H analyses. Our results document increased aridity before ~3.7 cal. ka BP, followed by two pronounced phases of warm and wet conditions from ~3.5–2.8 to ~2.3–1.5 cal. ka BP, and a strong increase in aridity since ~1.5 cal. ka BP. Phases of warmer and wetter conditions coincide with a negative North Atlantic Oscillation, which has been responsible for advecting moisture into the region by more southerly-displaced Westerlies and possibly favored the expansion of mobile nomadic pastoralism in the region.

Plain Language Summary Nomadic pastoralism is the dominant subsistence practice in the eastern Eurasian Steppe and Altai Region since the Late Bronze Age. Whether this had climatic reasons is one of the most intriguing question, because former climatic conditions are poorly understood in this important but understudied region. To address this issue, we established a hydrological record for the last ~4.2 ka from a high-altitude lake in the Mongolian Altai. Our findings provide evidence of exceptionally warm and wet conditions from ~3.5–2.8 and ~2.3–1.5 cal. ka BP. Those favorable climate conditions likely favored productive grasslands and the widespread dispersal of nomadic pastoralism in the eastern Eurasian Steppe and Altai Region.

1. Introduction

The semi-arid regions of the eastern Eurasian Steppe and the Altai Region are highly sensitive towards climate change and are expected to increasingly experience drought conditions by rising temperatures during the next decades (Batima et al., 2005; Dai, 2011). This sensitivity is mostly due to its continentality and complex climate forcing by the interplay of several large-scale atmospheric circulation patterns affecting moisture advection and precipitation variability (Aizen et al., 2001; D'Arrigo et al., 2000). While the cold and dry winter climate is controlled by the Siberian High, moisture and precipitation is mainly brought by the mid-latitude Westerlies and in the past to some extent by the low-latitude East Asian Summer Monsoon (EASM; Hoerling et al., 2001; Visbeck, 2002). However, the past evolution of those atmospheric circulation systems remains controversial, and little is known about their interactions and how they have affected climate variability in the region. Currently, paleoclimate information from the Altai Region is mainly derived from pollen-based vegetation reconstructions that mostly show more extensive forests and boreal woodlands before ~4 ka, and the dominance of steppe vegetation thereafter. This is generally interpreted to indicate warmer conditions with increased precipitation before ~4 ka, followed by colder conditions with decreased precipitation (Blyakharchuk et al., 2007; Brugger et al., 2018; Rudaya et al., 2009). However, the expansion of grasslands and steppes after ~4 ka BP could also be driven by intensified anthropogenic land-use, which is assumed to start with the introduction of mobile pastoralism from the Western Eurasian

steppe regions during the Early Bronze Age (~5 ka; de Barros Damgaard et al., 2018; Jeong et al., 2018). Nomadic population and pastoralism strongly expanded in the region during the Late Bronze Age between ~3.5 and 2.5 ka, which is linked to the introduction of horse-back riding and increased mobility (Taylor et al., 2019, 2020), and ultimately enabled the establishment of the famous Eurasian steppe empires of the Xiongnu (2.4–1.8 ka BP) and Mongols (0.8–0.3 ka BP; Honeychurch, 2013; Rogers, 2012). Increased livestock population and grazing during this time is indicated by coprophilous fungal spores, which grow on herbivore dung, and higher abundances of *Artemisia* (Brugger et al., 2018; Huang et al., 2018). However, climate-human-landscape interactions remain poorly understood, and one of the most intriguing questions is whether the rise and demise of nomadic empires had climatic reasons.

Therefore, novel and innovative proxies, that are more independent of anthropogenic land-use and land-cover change, are needed to complement pollen-based reconstructions and to shed new light on the Late Holocene climate history of the eastern Eurasian Steppe and Altai Region. Biomarkers are molecular fossils that are usually well-preserved in lake sediments, and analyzing their isotopic composition allow direct paleohydrological reconstructions. Leaf waxes such as long-chain n-alkanes for instance mainly record the δ^2H signal of precipitation (Häggi et al., 2019; Sachse et al., 2012; Strobel et al., 2020). Various fractionation processes along the pathway from the moisture source to the biosynthetic production of the leaf waxes can complicate the interpretation of leaf wax δ^2H records, with evapotranspirative enrichment being particularly relevant (Feakins & Sessions, 2010; Kahmen et al., 2013). However, for semi-arid Mongolia, we found that the apparent fractionation of n-C_{29} and n-C_{31}, that is, the isotopic difference between precipitation and the investigated compounds, remains relatively constant in topsoils, and so, these leaf wax n-alkanes primarily reflect the isotopic composition of precipitation (Struck et al., 2020). On the other hand, shorter n-alkanes, that is, n-C_{23}, are derived from aquatic plants (Ficken et al., 2000) and additionally record the evaporative enrichment of lake water. In semi-arid regions, like most parts of eastern Eurasia and the Altai Region, lakes are often endorheic and react highly sensitive to changes in precipitation/evaporation. Thus, the difference between aquatic versus terrestrial n-alkane δ^2H values is a valuable indicator for changes in lake water evaporation and increased/decreased evaporation rates in the lake's catchment (Aichner et al., 2019; Mügler et al., 2008; Toney et al., 2020).

Here, we present the first continuous high-resolution compound-specific n-alkane isotope record for the eastern Eurasian Steppe and the Altai Region. We have analyzed a lake sediment core from Lake Khar Nuur in the Mongolian Altai that covers the past 4.2 ka. The lake is situated at high altitude (2,486 m a.s.l.), has a small catchment with steep slopes and a para-glacial origin. Within the core from Lake Khar Nuur, we aim at reconstructing (a) the isotopic composition of past precipitation during the Late Holocene using δ^2H of leaf wax-derived n-C_{31} and (b) the evaporation history of the lake by additionally analyzing δ^2H of the aquatic n-C_{23}. A wide array of lake sediment proxies, including elemental composition, but also bulk $\delta^{13}C_{TOC}$ and $\delta^{15}N$, were used to describe and characterize the lake sediments in more detail, particularly to determine the lakes primary productivity that should mostly be temperature-driven in such a semi-arid and high-altitude environment.

2. Materials and Methods

2.1. Study Area

Lake Khar Nuur is a high-altitude lake situated at 2,486 m a.s.l. in the Mongolian Altai (48°37′22.9″N, 88°56′42.5″E; Figure 1) and has a para-glacial origin. Glacial advances from the south-western slopes of the Tsengel Khairkhan Massif during the Last Glacial Maximum (probably marine isotope stages 4 and 2; Gribenski et al., 2018) left prominent moraine lobes in the main valley and formed the endorheic Khar Nuur basin (Walther et al., 2017). The lake has a maximum water depth of 49.4 m and a relatively small hydrological catchment (44.8 km²) with steep slopes (Figure 1c; Strobel, Struck, et al., 2021). The geology of the catchment is mainly composed of friable black clay shales and granitic moraine deposits. Today's mean annual temperatures and precipitation at the nearest climate station Tolbo Sum (located ~90 km southeast of Lake Khar Nuur at 2,100 m a.s.l) is −2.4°C and 145.1 mm (climate data from 2009 to 2017; DWD Climate Data Center, last access date: 09.06.2020). Because of the high altitude and the low mean annual temperatures, the lake surface of Lake Khar Nuur is covered by ice for 8–9 month per year, which starts to thaw in
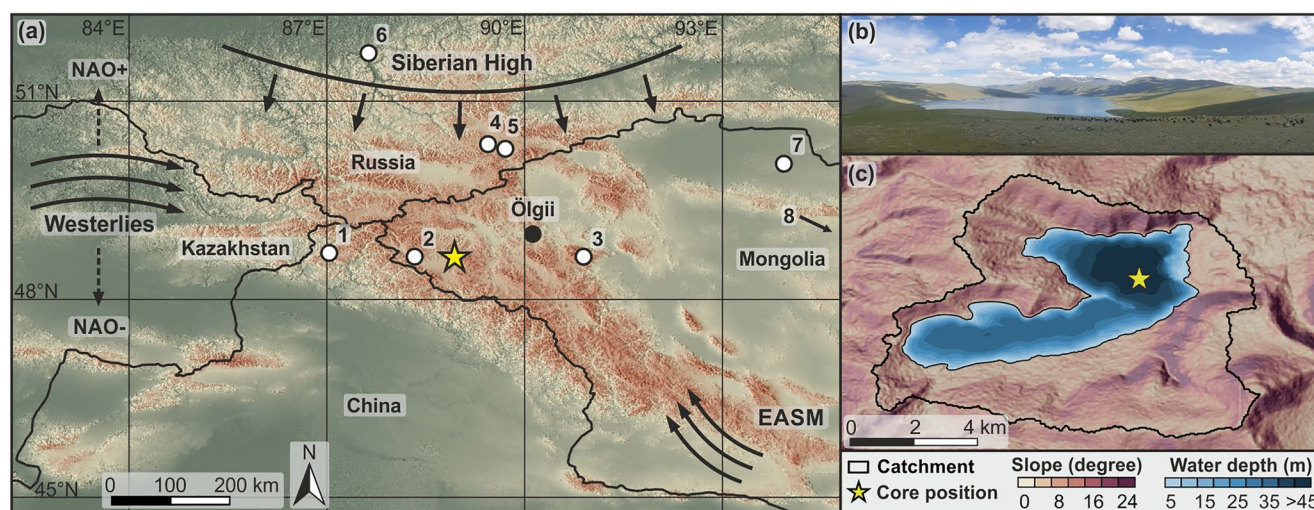
Figure 1. Overview of the study area. (a) Overview of the Altai Mountains with the major atmospheric circulation systems the Westerlies, the East Asian Summer Monsoon (EASM) and the Siberian High. Also displayed are changes in the North Atlantic Oscillation (NAO). The yellow star indicates the investigated site at Lake Khar Nuur. White dots refer to regional pollen records from the Altai: (1) Kanas Lake (Huang et al., 2018), (2) Hoton Nuur (Rudaya et al., 2009), (3) Tsambagarav ice core (Brugger et al., 2018), (4) Lake Grusha and (5) Lake Akkol (Blyakharchuk et al., 2007), (6) Lake Teletskoye (Rudaya et al., 2016), (7) Uvs Nuur basin (Rudaya et al., 2021) and (8) Bayan Nuur (Yang et al., 2020). (b) Picture of the southern part of Lake Khar Nuur and its catchment. (c) Slope map of the Khar Nuur catchment and lake bathymetry with the coring position indicated by the yellow star.

late June (Planet Team, last access date: 09.06.2020). For more information about the lake and its present spatial distribution of surface sediment compounds see Strobel, Struck, et al. (2021).

2.2. Sediment Core and Chronology

For this study, a 141 cm long gravity core was retrieved in 2018 from the deepest part of the Khar Nuur basin using an Uwitec gravity corer. The core was split and photographed at the Friedrich Schiller University Jena (see Text S1 in Supporting Information S1 for detailed lithostratigraphic information). One half was analyzed for elemental composition by an X-ray fluorescence (XRF) core scanner (Avaatech) at 5 mm resolution at the Eawag Aquatic Institute, Switzerland. The other half of the core was subsampled at 1 cm intervals, freeze-dried and homogenized for further analyses. The chronology of the core is based on ^{14}C-measurements of twelve bulk organic carbon samples, eight aquatic macrofossil samples and one ostracod shell sample, carried out at the Laboratory for the Analysis of Radiocarbon with AMS (LARA AMS) of the University of Bern, Switzerland (Szidat et al., 2014; for detailed analytical and calibration information, see Text S1 in Supporting Information S1). Additionally, we ^{14}C-dated one surface sediment bulk organic carbon sample and a modern water plant in a previous study (Strobel, Struck, et al., 2021) to account for possible terrestrial "pre-aging" and "hardwater" effects. The surface sediment bulk organic carbon sample gave a slight reservoir effect with a mean ^{14}C-age of 129 ± 85 cal. BP (age range = [−7]–278 cal. BP [95.4%]), but no hardwater effect was indicated by modern ^{14}C-ages of the modern water plant (see Text S1 and Table S1 in Supporting Information S1 for ^{14}C-results). Based on the ^{14}C-dating results, Bayesian age modeling was applied using the Bacon 2.3.4 package in R (Blaauw & Christen, 2011) to establish an age-depth model that gives the timing of sediment deposition. The slight reservoir effect was subtracted from the bulk organic carbon ^{14}C-ages during age-depth modeling. Since four bulk organic carbon samples gave ages that are too old and overestimate their "true" timing of deposition, we excluded them from the age-depth model in a second iteration.

2.3. Geochemical Analyses and Productivity Index

Geochemical analyses – namely XRF core scanning, CN analyses and their stable isotopes ($\delta^{13}C_{TOC}$ and $\delta^{15}N$) and biogenic silica (BiSi) – were carried out to characterize the lake sediment compounds (see Text S2 in Supporting Information S1 for detailed analytical information and results) and compile the Productivity

Index (PI). For the calculation of the PI we performed a Z-transformation of the elemental ratio log (Ca/Ti), N, TOC, $\delta^{13}C_{TOC}$, $\delta^{15}N$ and BiSi to normalize them and generate dimensionless values. The PI was then calculated as follows:

$$PI = \frac{\left(\log\left(Ca/Ti\right) + N + TOC + \delta^{13}C_{TOC} + \delta^{15}N + BiSi \right)}{6}$$

2.4. Compound-Specific Biomarker δ^2H Analyses

For biomarker analyses, free total lipids were extracted from sediments by Ultrasonic extraction with dichloromethane (DCM)/methanol (MeOH; 9:1, v/v) for 15 min at three cycles. The total lipid extract was separated over Aminopropyl pipette columns (Supleco, 45 μm) into fractions of different polarity. The apolar fraction including the *n*-alkanes was eluted with hexane and further purified over coupled silver nitrate (AgNO$_3$)—zeolite pipette columns due to coeluting compounds. Identification and quantification of the *n*-alkanes was carried out on an Agilent 7890B gas-chromatograph equipped with an Agilent HP5MS column (30 m, 320 μm, 0.25 μm film thickness) and a flame ionization detector, relative to external *n*-alkane standards (*n*-C$_{21}$–*n*-C$_{40}$). Compound-specific hydrogen isotopes of the *n*-alkanes were analyzed using an Isoprime visION isotope ratio mass spectrometer coupled via a GC5 pyrolysis-combustion interface to a gas chromatograph (Agilent 7890B). The GC5 operated in pyrolysis mode for the δ^2H analyses with a chrome reactor at 1,050°C. Samples were injected splitless and measured as triplicates. The analytical precision was checked twice after six injections by certified external *n*-alkane standards with a known isotopic composition (Arndt Schimmelmann, University of Indiana). The H^{3+}-correction factor was checked regularly and gave values of 4.12 ± 0.04. The hydrogen isotopic composition is given in its delta notation in permill, that is, as δ^2H vs. the Vienna Standard Mean Ocean Water (VSMOW). $\Delta_{aq\text{-}terr}$—the offset between the aquatic and terrestrial *n*-alkanes—followed the calculation of Aichner et al. (2019) and was calculated as follows:

$$\Delta_{aq\text{-}terr} = 1000 * \left(\left(\frac{n-C_{23} + 1000}{n-C_{31} + 1000} \right) - 1 \right)$$

3. Results

The 141 cm long sediment core from Lake Khar Nuur consists of well laminated silty sediments (silt content is generally >75% and the median grain size only slightly varies between 2.4 and 12.2 μm) and is characterized by colors ranging from dominantly brown and blackish dark to blueish gray. Bayesian age modeling of Lake Khar Nuur sediments gave a modeled basal median age of 4.2 cal. ka BP (Figure 2a). Most ^{14}C-ages are in stratigraphic order, except four ages at 90, 40, 30 and 20 cm sediment depth, that are slightly too old and overestimate their timing of sediment deposition (Figure 2a). In Figure 2b, the normalized and dimensionless PI is additionally shown with the log (Ca/Ti) ratio because it was measured in higher resolution (0.5 cm) and agrees well with the PI. Both proxies show phases of increased productivity (higher values) which coincides with brown to blackish dark sediments, while reduced productivity (lower values) coincides with blueish gray sediments (Figures 2a and 2b). Detailed lithostratigraphic and geochemical information as well as ^{14}C-data are provided as Text S1 and S2 in Supporting Information S1. Compound-specific δ^2H values of the analyzed *n*-alkanes range from −226.3 ± 0.9 to −199.3 ± 1.4‰ for the terrestrial *n*-C$_{31}$ and from −210.2 ± 1.8 to −136.9 ± 0.9‰ for the aquatic *n*-C$_{23}$ (Figure 2c). The offset between the aquatic *n*-C$_{23}$ and the terrestrial *n*-C$_{31}$ ($\Delta_{aq\text{-}terr}$) ranges from −1.5 to 86.4‰ (Figure 2c).

4. Discussion

The laminated fine-grained silty sediments from Lake Khar Nuur encompass the past ~4.2 cal. ka based on the modeled basal median ^{14}C-age of 4.2 cal. ka BP (Figure 2a). Although dating semi-arid lake sediments can be complicated because terrestrial macrofossils are often absent and reworked old carbon can contribute to the ^{14}C-age, our dating approach of bulk organic carbon and aquatic macrofossil ^{14}C-ages yield stratigraphic consistent ages that agree well with each other (more detailed information about the potential reservoir effects are given in Text S1 in Supporting Information S1).
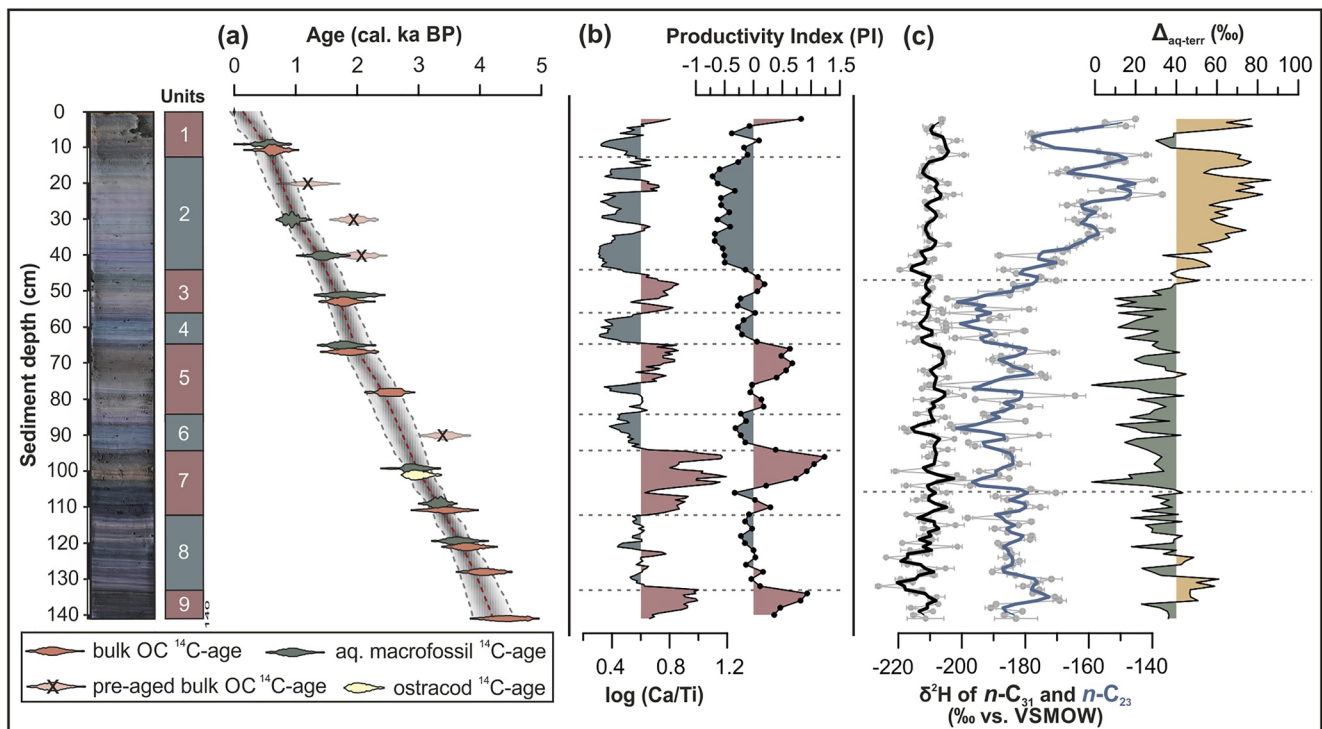
Figure 2. Chronostratigraphy and depth profiles of Khar Nuur sediments. (a) Age-depth model of the Khar Nuur sediment core based on bulk organic carbon (OC), aquatic macrofossil and ostracod ^{14}C-ages (see Text S1 and Table S1 in Supporting Information S1 for more details). (b) log (Ca/Ti) ratio and PI, which is a normalized and dimensionless ratio of the biogeochemical proxies log (Ca/Ti), TOC, N, $\delta^{13}C_{TOC}$, $\delta^{15}N$ and biogenic silica (BiSi). (c) Compound-specific δ^2H of the terrestrial n-C$_{31}$, the aquatic n-C$_{23}$ and $\Delta_{aq-terr}$, which is the offset between the aquatic and terrestrial n-alkanes.

Lake sediment proxies that are ultimately compiled in the Productivity Index (PI) reveal phases of increased lake primary productivity in the brown and blackish dark sediments and reduced productivity in the blue-ish gray sediments (Figures 2a and 2b and Text S2 in Supporting Information S1). Since PI and log (Ca/Ti) ratio agree well with each other, we will use and show the log (Ca/Ti) ratio exemplarily for interpretation because of the higher resolution (0.5 mm). Although it is notable that the used lake sediment proxies are also an indicator for allochthonous and autochthonous sedimentary sources (Strobel, Struck, et al., 2021), they mostly indicate variations in primary productivity of the high-altitude Lake Khar Nuur, that is mainly controlled by the growing season. Such a temperature dependency has been reported from high-latitude and high-altitude lakes (Mischke et al., 2010; Willemse & Törnqvist, 1999) because air temperatures control the duration of the ice cover and thus the open water growing season of aquatic producers. Therefore, primary productivity is strongly increased during warmer summers with higher air temperatures that results in longer ice-free periods and improved light conditions, gas exchange and circulation within the water body (Willemse & Törnqvist, 1999). Accordingly, higher growing season temperatures are indicated by higher values of the lake sediment proxies including the log (Ca/Ti) ratio in Lake Khar Nuur before ∼4.0 cal. ka BP, from ∼3.5 to 2.8 cal. ka BP and from ∼2.3 to 1.5 cal. ka BP. Lower growing season temperatures occur at ∼3.5, ∼2.8 and ∼2.4 cal. ka BP, and during the last ∼1.5 cal. ka BP, as indicated by lower values (Figure 3b). Changes in growing season temperatures at Lake Khar Nuur seem to be driven by total solar irradiance (TSI). The two pronounced phases of increased growing season temperatures from ∼3.5 to 2.8 and ∼2.3 to 1.5 cal. ka BP coincide with increased TSI (Steinhilber et al., 2012; Figures 3b and 3c). The phase of increased growing season temperatures from ∼2.3 to 1.5 cal. ka BP includes the Roman Warm Period (RWP) that likewise appears as a warm period in our record. Colder conditions with reduced primary productivity due to increased ice periods occur at Lake Khar Nuur during minima in TSI. Abrupt changes to lower growing season temperatures coincide well with TSI minima at ∼3.5, ∼2.8 and ∼2.4 ka BP (Figures 3b and 3c). Substantially and long-lasting lower growing season temperatures at Lake Khar Nuur start at ∼1.5 cal. ka BP and agree well with the solar minimum that has been previously reported as a substantial cold phase in the Altai Region by tree rings and corresponds to the Late Antique Little Ice Age (LALIA; Büntgen
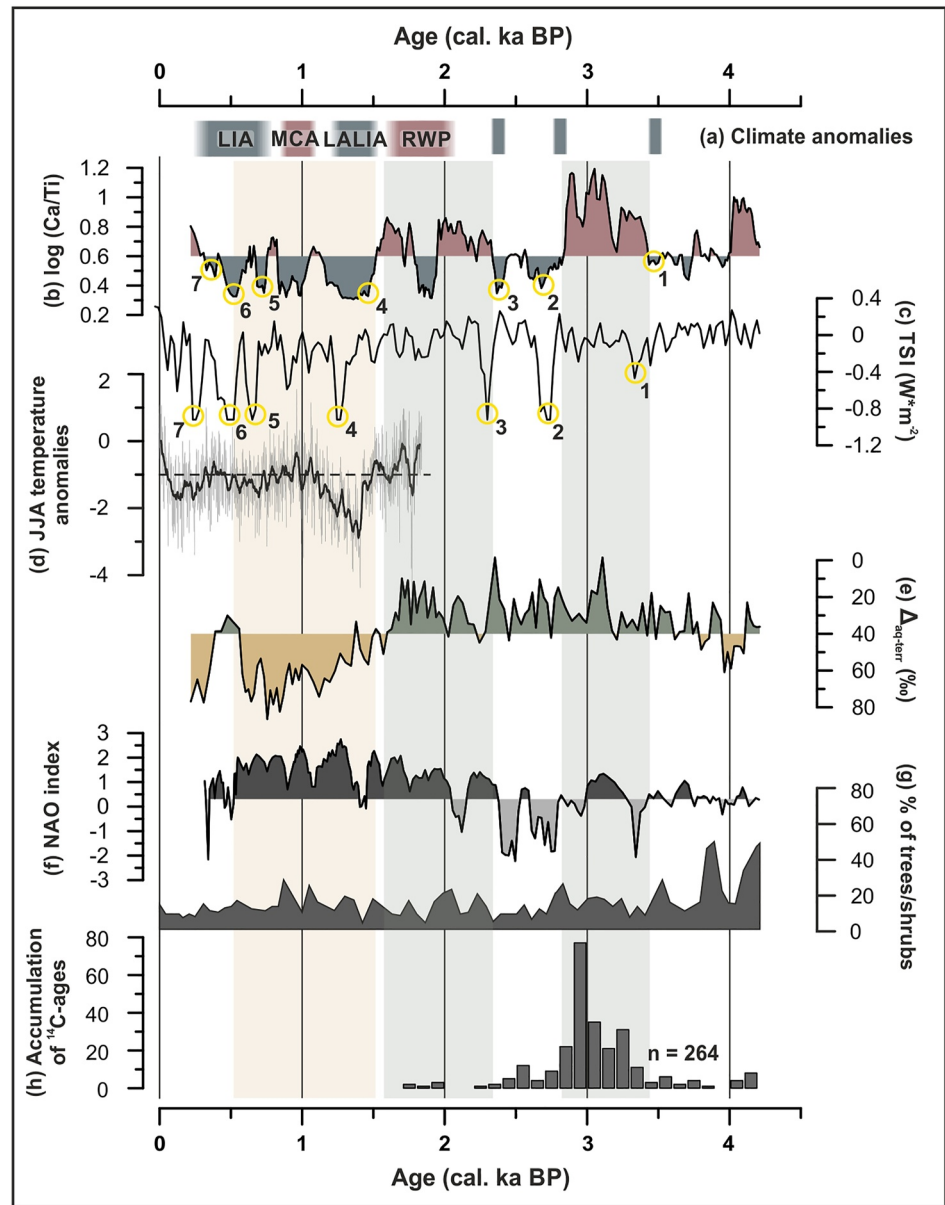
Figure 3. Late Holocene temperature and hydrological changes. (a) Late Holocene climate anomalies after Büntgen et al. (2016), LIA, Little Ice Age; MCA, Medieval Climate Anomaly; LALIA, Late Antique Little Ice Age; RWP, Roman Warm Period; and abrupt Holocene cooling events at 3.4, 2.8 and 2.4 ka BP. (b) log (Ca/Ti) ratio that reflects the productivity-based growing season temperature from Lake Khar Nuur. (c) Total solar irradiance (Steinhilber et al., 2012). (d) Reconstructed summer temperatures from the Altai (Büntgen et al., 2016). (e) Moisture availability and evaporation in the Khar Nuur catchment ($\Delta_{aq\text{-}terr}$). (f) The North Atlantic Oscillation Index (NAO; Olsen et al., 2012). (g) Tsambagarav ice core pollen reconstruction (Brugger et al., 2018). (h) Accumulation of Bronze Age ^{14}C-ages from burial mounds and monument constructions, modified after Huang et al. (2021) and Taylor et al. (2019, 2020, 2021).

et al., 2016; Figures 3b–3d). Colder conditions prevail during the Medieval Climate Anomaly (MCA; ~1.1–0.8 ka BP) and the Little Ice Age (LIA; ~0.8–0.1 ka BP) at Lake Khar Nuur. Colder conditions recorded in our record during the MCA are exceptional in the region since other regional paleorecords mostly report warmer conditions during this time (e.g., Uvs Nuur basin, Rudaya et al., 2021; Bayan Nuur, Yang et al., 2020; Lake Teletskoye, Rudaya et al., 2016). However, we have to emphasize that some uncertainties might exist in the upper 45 cm of the sediment core because of a potentially slightly increased "hardwater" effect during

this time by longer ice periods (Figures 2a and 2b). Thus, considering dating- and modeling uncertainties, those sediments might also correspond to the LIA instead of the LALIA and MCA.

Distinct hydrological changes are recorded in the Khar Nuur sediments by compound-specific δ^2H variability, which is on the order of ~25‰ for the terrestrial $n\text{-}C_{31}$ and ~70‰ for the aquatic $n\text{-}C_{23}$. While δ^2H of $n\text{-}C_{31}$ only show minor changes over the sediment core, δ^2H of $n\text{-}C_{23}$ is enriched below 105 cm (i.e., before ~3.2 cal. ka BP) and above 45 cm (i.e., after ~1.5 cal. ka BP), and depleted inbetween (i.e., from ~3.2 to ~1.5 cal. ka BP; Figure 2c; see Figure S3 in Supporting Information S1 for the age relationship of δ^2H of $n\text{-}C_{31}$ and $n\text{-}C_{23}$). The different observed variabilities in δ^2H of terrestrial and aquatic n-alkanes are due to the different water sources used for biosynthesis. δ^2H of the terrestrial $n\text{-}C_{31}$ mostly reflects the isotopic signal of the local growing season precipitation that becomes incorporated by the plant (Sachse et al., 2012). For semi-arid Eurasia, such a relationship was proven by the calibration study of Struck et al. (2020), and even suggested for the Khar Nuur catchment from topsoil and surface sediment samples by Strobel, Zech, et al. (2021). In contrast, δ^2H of the aquatic $n\text{-}C_{23}$ reflects the isotopic signal of the lake water (Sachse et al., 2004), and especially in endorheic semi-arid lakes, lake water is highly sensitive to changes in precipitation/evaporation. Lake water can therefore be strongly modulated by evaporative enrichment, which holds especially true for Lake Khar Nuur, where such a strong evaporative enrichment is shown by surface sediment samples (Strobel, Zech, et al., 2021). Consequently, the difference between the terrestrial and aquatic δ^2H ($\Delta_{\text{aq-terr}}$) is a valuable indicator for evaporative enrichment and more arid conditions in semi-arid lakes and Lake Khar Nuur (Aichner et al., 2019; Mügler et al., 2008; Strobel, Zech, et al., 2021). The $\Delta_{\text{aq-terr}}$ is high before ~3.7 cal. ka BP and very high from ~1.5 to 0.5 cal. ka BP. In contrast, evaporation is low between ~3.5 and 1.5 cal. ka BP, indicating wetter conditions in the Khar Nuur catchment (Figure 3e). Those wetter conditions and decreased evaporation rates in the Khar Nuur catchment correspond well with a negative phase of the North Atlantic Oscillation (NAO) during this time (Figures 3e and 3f). The position of the NAO influences the strength and direction of the Westerlies (Olsen et al., 2012) and it was suggested that precipitation availability in the eastern Eurasian Steppe and the Altai Region is mainly supplied during negative NAO phases. During a negative NAO, the Westerlies are migrated southward and bring increased winter precipitation to the region from the southern part of the North Atlantic and the Mediterranean Sea (Lan et al., 2021). This inverse relationship of increased winter precipitation during negative NAO phases was suggested by modeled modern air mass trajectories by Wolff et al. (2017), but also suggested for the past ~4 ka for the Tienshan Mountains (Lan et al., 2020), the Siberian Altai (Aizen et al., 2001) and central Mongolia (Yang et al., 2020). Dryer conditions and strongly increased evaporation rates in the Khar Nuur catchment after ~1.5 cal. ka BP correspond to a positive NAO phase where the Westerlies have migrated northward and probably supply moisture to southern Siberia and the Russian Plain but not to the Altai Region (Feurdean et al., 2019; Wang & Feng, 2013; Figure 3f). However, we have to mention that precipitation at our site is not neccessary solely brought by the Westerlies, precipitation can also be derived from local sources in the lowlands during convective events.

Compared to the existing paleoclimate records in the Altai Region that are mostly based on pollen records, warmer and wetter conditions as indicated by our record from ~3.5 to 1.5 cal. ka BP partly disagrees with previous investigations (Figures 3b and 3e). Overall, existing paleoclimate studies draw a diverse picture of the Late Holocene climate. A successive drying trend since ~4 ka BP is suggested by the regional moisture index of Wang and Feng (2013), and a decline of forest pollen and expansion of herbaceous steppe vegetation since ~4 ka BP was reported for example from the Tsambagarav ice core (Brugger et al., 2018), Hoton Nuur (Rudaya et al., 2009), Lake Akkol and Grusha (Blyakharchuk et al., 2007) and Lake Kanas (Huang et al., 2018; Figure 3g; see Figure 1 for locations). In contrast, Klinge and Sauer (2019) suggested in their extensive review a change to wetter conditions in some records at ~3 ka, which is supported by warmer conditions and forest expansion at Lake Teletskoye (Rudaya et al., 2016) and in the near surroundings to our record in the Dayan Nuur region (Unkelbach et al., 2019). However, several studies also pointed out that especially since ~3 ka anthropogenic land-use might have played an important role in landscape shaping. Declining forest pollen are often accompanied by higher abundances of the fungi spores *Coprophilous* and *Sporormiella* that grow on herbivore dung (Brugger et al., 2018; Unkelbach et al., 2019), but also by higher abundances of *Artemisia* which are interpreted as a result of forest clearing and overgrazing (Fowell et al., 2003; Huang et al., 2018; Tian et al., 2013).

Therefore, differences between some pollen reconstructions and our more independent isotope-based reconstructions might be due to the beginning of anthropogenic activity in the region. Especially the pronounced period of warm and wet conditions between ∼3.5 and 2.8 cal. ka BP falls into a period where substantial economic and societal transitions took place in the eastern Eurasian Steppe and Altai Region. While migration of early pastoralists into the region took place during the Early Bronze Age ∼5.3 ka BP (de Barros Damgaard et al., 2018; Huang et al., 2021; Jeong et al., 2018), ^{14}C-ages of burial mounds and monument constructions mostly accumulate during the Late Bronze Age from ∼3.2 to 2.8 ka BP (Taylor et al., 2019; Figure 3h). At the same time, horses became important for mobility, diet and ritual assemblages at ∼3.2 ka BP, which might have resulted in a widespread population dispersal in the region (Taylor et al., 2020). Only recently, Taylor et al. (2021) found evidence that early pastoralists were present in the surroundings of our study area at the northern slopes of the Tsengel Khairkhan Massif at the end of the 4th and beginning of the 3rd millennium BP. Therefore, we suggest that pronounced warm and wet conditions between ∼3.5 and 2.8 cal. ka BP might have favored the widespread dispersal of mobile horse-borne pastoralism in the Altai Region and across the eastern Eurasian Steppe.

5. Conclusions

Our study present the first continuous high-resolution compound-specific n-alkane isotope record for the eastern Eurasian Steppe and the Altai Region. Our 4.2 ka paleoclimate record gave the following results:

1. Lake sediment proxies ultimately compiled in the Productivity index reveal alternating phases of increased and decreased lake primary productivity, which is mostly controlled by the growing season temperatures and the duration of ice cover in the high-altitude Lake Khar Nuur. Higher growing season temperatures occur before ∼4.0 cal. ka BP, from ∼3.5 to 2.8 cal. ka BP and from ∼2.3 to 1.5 cal. ka BP, whereas temperatures are low at ∼3.5, ∼2.8 and ∼2.4 cal. ka BP, and during the last ∼1.5 cal. ka BP. Growing season temperatures and the duration of ice cover are mainly driven by total solar irradiance.
2. Distinct hydrological differences are recorded by compound-specific δ^2H of terrestrial (n-C$_{31}$) and aquatic (n-C$_{23}$) alkanes. The $\Delta_{\text{aq-terr}}$, which is the offset between the terrestrial and aquatic δ^2H and our indicator for evaporative enrichment and more arid conditions, indicate that evaporation is high in the Khar Nuur catchment before ∼3.7 cal. ka BP and from ∼1.5 to 0.5 cal. ka BP. In contrast, evaporation is low from ∼3.5 to 1.6 cal. ka BP, which is mostly due to increased precipitation and a greater moisture availability during a negative NAO phase.
3. The two pronounced phases of warmer and wetter conditions in our record from ∼3.5 to 2.8 cal. ka BP and from ∼2.3 to 1.5 cal. ka BP are exceptional in the eastern Eurasian Steppe and the Altai Region, and especially the former phase falls into a period where mobile nomadic pastoralism become widely dispersed into the region. We therefore suggest that this widespread dispersal might be favored by those pronounced warm and humid conditions during the Late Holocene at ∼3 ka.

Data Availability Statement

The data used in this study were published open access by Bliedtner et al. (2021) and are available on PANGAEA via https://doi.org/10.1594/PANGAEA.936512.

References

Aichner, B., Makhmudov, Z., Rajabov, I., Zhang, Q., Pausata, F. S. R., Werner, M., et al. (2019). Hydroclimate in the Pamirs was driven by changes in precipitation-evaporation seasonality since the last glacial period. *Geophysical Research Letters*, *46*(23), 13972–13983. https://doi.org/10.1029/2019GL085202

Aizen, E., Aizen, V., Melack, J., Nakamura, T., & Ohta, T. (2001). Precipitation and atmospheric circulation patterns at mid-latitudes of Asia. *International Journal of Climatology*, *21*(5), 535–556. https://doi.org/10.1002/joc.626

Batima, P., Natsagdorj, L., Gombluudev, P., & Erdenetsetseg, B. (2005). Observed climate change in Mongolia. *Assessment of Impact and Adaptation Climate Change Working Paper*, *12*, 1–26.

Blaauw, M., & Christen, J. A. (2011). Flexible paleoclimate age-depth models using an autoregressive gamma process. *Bayesian Analysis*, *6*(3), 457–474. https://doi.org/10.1214/11-BA618

Bliedtner, M., Struck, J., Strobel, P., Salazar, G., Szidat, S., Bazarradnaa, E., et al. (2021). *High-resolution biomarker isotope and geochemical data for the ∼4.2 ka sediment core from Lake Khar Nuur, Mongolian Altai*. PANGAEA. https://doi.org/10.1594/PANGAEA.936512

Blyakharchuk, T. A., Wright, H. E., Borodavko, P. S., van der Knaap, W. O., & Ammann, B. (2007). Late Glacial and Holocene vegetational history of the Altai Mountains (southwestern Tuva Republic, Siberia). *Palaeogeography, Palaeoclimatology, Palaeoecology*, *245*(3–4), 518–534. https://doi.org/10.1016/j.palaeo.2006.09.010

Brugger, S. O., Gobet, E., Sigl, M., Osmont, D., Papina, T., Rudaya, N., et al. (2018). Ice records provide new insights into climatic vulnerability of Central Asian forest and steppe communities. *Global and Planetary Change*, *169*, 188–201. https://doi.org/10.1016/j.gloplacha.2018.07.010

Büntgen, U., Myglan, V. S., Ljungqvist, F. C., McCormick, M., Di Cosmo, N., Sigl, M., et al. (2016). Cooling and societal change during the late antique little ice age from 536 to around 660 AD. *Nature Geoscience*, *9*(3), 231–236. https://doi.org/10.1038/NGEO2652

Dai, A. (2011). Drought under global warming: A review. *Climate Change*, *2*(1), 45–65. https://doi.org/10.1002/wcc.81

D'Arrigo, R., Jacoby, G., Pederson, N., Frank, D., Buckley, B., Nachin, B., et al. (2000). Mongolian tree-rings, temperature sensitivity and reconstructions of Northern Hemisphere temperature. *The Holocene*, *10*(6), 669–672.

de Barros Damgaard, P., Martiniano, R., Kamm, J., Moreno-Mayar, J. V., Kroonen, G., Peyrot, M., et al. (2018). The first horse herders and the impact of early Bronze Age steppe expansions into Asia. *Science*, *360*, 6396. https://doi.org/10.1126/science.aar7711

Feakins, S. J., & Sessions, A. L. (2010). Controls on the D/H ratios of plant leaf waxes in an arid ecosystem. *Geochimica et Cosmochimica Acta*, *74*(7), 2128–2141. https://doi.org/10.1016/j.gca.2010.01.016

Feurdean, A., Gałka, M., Florescu, G., Diaconu, A.-C., Tanţău, I., Kirpotin, S., et al. (2019). 2000 years of variability in hydroclimate and carbon accumulation in western Siberia and the relationship with large-scale atmospheric circulation: A multi-proxy peat record. *Quaternary Science Reviews*, *226*, 105948. https://doi.org/10.1016/j.quascirev.2019.105948

Ficken, K. J., Li, B., Swain, D. L., & Eglinton, G. (2000). An n-alkane proxy for the sedimentary input of submerged/floating freshwater aquatic macrophytes. *Organic Geochemistry*, *31*(7–8), 745–749. https://doi.org/10.1016/S0146-6380(00)00081-4

Fowell, S. J., Hansen, B. C., Peck, J. A., Khosbayar, P., & Ganbold, E. (2003). Mid to late Holocene climate evolution of the lake Telmen basin, north central Mongolia, based on palynological data. *Quaternary Research*, *59*(3), 353–363. https://doi.org/10.1016/S0033-5894(02)00020-0

Gribenski, N., Jansson, K. N., Preusser, F., Harbor, J. M., Stroeven, A. P., Trauerstein, M., et al. (2018). Re-evaluation of MIS 3 glaciation using cosmogenic radionuclide and single grain luminescence ages, Kanas Valley, Chinese Altai. *Journal of Quaternary Science*, *33*(1), 55–67. https://doi.org/10.1002/jqs.2998

Häggi, C., Eglinton, T. I., Zech, W., Sosin, P., & Zech, R. (2019). A 250 ka leaf-wax δD record from a loess section in Darai Kalon, Southern Tajikistan. *Quaternary Science Reviews*, *208*, 118–128. https://doi.org/10.1016/j.quascirev.2019.01.019

Hoerling, M. P., Hurrell, J. W., & Xu, T. (2001). Tropical origins for recent North Atlantic climate change. *Science*, *292*(5514), 90–92. https://doi.org/10.1126/science.1058582

Honeychurch, W. (2013). The nomad as state builder: Historical theory and material evidence from Mongolia. *Journal of World Prehistory*, *26*(4), 283–321. https://doi.org/10.1007/s10963-013-9069-2

Huang, X., Peng, W., Rudaya, N., Grimm, E. C., Chen, X., Cao, X., et al. (2018). Holocene vegetation and climate dynamics in the Altai Mountains and surrounding areas. *Geophysical Research Letters*, *45*(13), 6628–6636. https://doi.org/10.1029/2018GL078028

Huang, X., Xiang, L., Lei, G., Sun, M., Qiu, M., Storozum, M., et al. (2021). Sedimentary pediastrum record of middle-late Holocene temperature change and its impacts on early human culture in the desert-oasis area of northwestern China. *Quaternary Science Reviews*, *265*, 107054. https://doi.org/10.1016/j.quascirev.2021.10705

Jeong, C., Wilkin, S., Amgalantugs, T., Bouwman, A. S., Taylor, W. T. T., Hagan, R. W., et al. (2018). Bronze Age population dynamics and the rise of dairy pastoralism on the eastern Eurasian steppe. *Proceedings of the National Academy of Sciences of the United States of America*, *115*(48), E11248–E11255. https://doi.org/10.1073/pnas.1813608115

Kahmen, A., Schefuß, E., & Sachse, D. (2013). Leaf water deuterium enrichment shapes leaf wax n-alkane δD values of angiosperm plants I: Experimental evidence and mechanistic insights. *Geochimica et Cosmochimica Acta*, *111*, 39–49. https://doi.org/10.1016/j.gca.2012.09.003

Klinge, M., & Sauer, D. (2019). Spatial pattern of late glacial and holocene climatic and environmental development in Western Mongolia—A critical review and synthesis. *Quaternary Science Reviews*, *210*, 26–50. https://doi.org/10.1016/j.quascirev.2019.02.020

Lan, J., Wang, T., Dong, J., Kang, S., Cheng, P., Zhou, K., et al. (2021). The influence of ice sheet and solar insolation on Holocene moisture evolution in northern Central Asia. *Earth-Science Reviews*, *217*, 103645. https://doi.org/10.1016/j.earscirev.2021.103645

Lan, J., Zhang, J., Cheng, P., Ma, X., Ai, L., Chawchai, S., et al. (2020). Late Holocene hydroclimatic variation in central Asia and its response to mid-latitude Westerlies and solar irradiance. *Quaternary Science Reviews*, *238*, 106330. https://doi.org/10.1016/j.quascirev.2020.106330

Mischke, S., Rajabov, I., Mustaeva, N., Zhang, C., Herzschuh, U., Boomer, I., et al. (2010). Modern hydrology and late Holocene history of Lake Karakul, eastern Pamirs (Tajikistan): A reconnaissance study. *Palaeogeography, Palaeoclimatology, Palaeoecology*, *289*(1–4), 10–24. https://doi.org/10.1016/j.palaeo.2010.02.004

Mügler, I., Sachse, D., Werner, M., Xu, B., Wu, G., Yao, T., & Gleixner, G. (2008). Effect of lake evaporation on δD values of lacustrine n-alkanes: A comparison of Nam Co (Tibetan Plateau) and Holzmaar (Germany). *Organic Geochemistry*, *39*(6), 711–729. https://doi.org/10.1016/j.orggeochem.2008.02.008

Olsen, J., Anderson, N. J., & Knudsen, M. F. (2012). Variability of the North Atlantic oscillation over the past 5,200 years. *Nature Geoscience*, *5*(11), 808–812. https://doi.org/10.1038/ngeo1589

Rogers, J. D. (2012). Inner Asian states and empires: Theories and synthesis. *Journal of Archaeological Research*, *20*(3), 205–256. https://doi.org/10.1007/s10814-011-9053-2

Rudaya, N., Nazarova, L., Frolova, L., Palagushkina, O., Soenov, V., Cao, X., et al. (2021). The link between climate change and biodiversity of lacustrine inhabitants and terrestrial plant communities of the Uvs Nuur Basin (Mongolia) during the last three millennia. *The Holocene*, https://doi.org/10.1177/09596836211019093

Rudaya, N., Nazarova, L., Novenko, E., Andreev, A., Kalugin, I., Daryin, A., et al. (2016). Quantitative reconstructions of mid- to late Holocene climate and vegetation in the north-eastern Altai Mountains recorded in lake Teletskoye. *Global and Planetary Change*, *141*, 12–24. https://doi.org/10.1016/j.gloplacha.2016.04.002

Rudaya, N., Tarasov, P., Dorofeyuk, N., Solovieva, N., Kalugin, I., Andreev, A., et al. (2009). Holocene environments and climate in the Mongolian Altai reconstructed from the Hoton-Nur pollen and diatom records: A step towards better understanding climate dynamics in Central Asia. *Quaternary Science Reviews*, *28*(5–6), 540–554. https://doi.org/10.1016/j.quascirev.2008.10.013

Sachse, D., Billault, I., Bowen, G. J., Chikaraishi, Y., Dawson, T. E., Feakins, S. J., et al. (2012). Molecular paleohydrology: Interpreting the hydrogen-isotopic composition of lipid biomarkers from photosynthesizing organisms. *Annual Review of Earth and Planetary Sciences*, *40*(1), 221–249. https://doi.org/10.1146/annurev-earth-042711-105535

Sachse, D., Radke, J., & Gleixner, G. (2004). Hydrogen isotope ratios of recent lacustrine sedimentary n-alkanes record modern climate variability. *Geochimica et Cosmochimica Acta*, *68*(23), 4877–4889. https://doi.org/10.1016/j.gca.2004.06.004

Steinhilber, F., Abreu, J. A., Beer, J., Brunner, I., Christl, M., Fischer, H., et al. (2012). 9,400 years of cosmic radiation and solar activity from ice cores and tree rings. *Proceedings of the National Academy of Sciences of the United States of America*, *109*(16), 5967–5971. https://doi.org/10.1073/pnas.1118965109

Strobel, P., Haberzettl, T., Bliedtner, M., Struck, J., Glaser, B., Zech, M., et al. (2020). The potential of $\delta^2H_{\text{n-alkanes}}$ and $\delta^{18}O_{\text{sugar}}$ for paleoclimate reconstruction—A regional calibration study for South Africa. *The Science of the Total Environment*, *716*, 137045. https://doi.org/10.1016/j.scitotenv.2020.137045

Strobel, P., Struck, J., Zech, R., & Bliedtner, M. (2021). The spatial distribution of sedimentary compounds and their environmental implications in surface sediments of Lake Khar Nuur (Mongolian Altai). *Earth Surface Processes and Landforms*, *55*, 319–625. https://doi.org/10.1002/esp.5049

Strobel, P., Zech, R., Struck, J., Bazarradnaa, E., Zech, M., & Bliedtner, M. (2021). Precipitation and lake water evaporation recorded by terrestrial and aquatic *n*-alkane δ^2H isotopes in Lake Khar Nuur, Mongolia. *Earth and Space Science*. https://doi.org/10.1002/essoar.10507650.1

Struck, J., Bliedtner, M., Strobel, P., Bittner, L., Bazarradnaa, E., Andreeva, D., et al. (2020). Leaf waxes and hemicelluloses in topsoils reflect the δ^2H and $\delta^{18}O$ isotopic composition of precipitation in Mongolia. *Frontiers in Earth Science*, *8*. https://doi.org/10.3389/feart.2020.00343

Szidat, S., Salazar, G. A., Vogel, E., Battaglia, M., Wacker, L., Synal, H.-A., et al. (2014). ^{14}C analysis and sample preparation at the New Bern Laboratory for the analysis of radiocarbon with AMS (LARA). *Radiocarbon*, *56*(2), 561–566. https://doi.org/10.2458/56.17457

Taylor, W., Hart, I., Pan, C., Bayarsaikhan, J., Murdoch, J., Caspari, G., et al. (2021). High altitude hunting, climate change, and pastoral resilience in eastern Eurasia. *Scientific Reports*, *11*(1), 14287. https://doi.org/10.1038/s41598-021-93765-w

Taylor, W., Wilkin, S., Wright, J., Dee, M., Erdene, M., Clark, J., et al. (2019). Radiocarbon dating and cultural dynamics across Mongolia's early pastoral transition. *PLoS One*, *14*(11), e0224241. https://doi.org/10.1371/journal.pone.0224241

Taylor, W. T. T., Clark, J., Bayarsaikhan, J., Tuvshinjargal, T., Jobe, J. T., Fitzhugh, W., et al. (2020). Early pastoral economies and herding transitions in Eastern Eurasia. *Scientific Reports*, *10*(1), 1001. https://doi.org/10.1038/s41598-020-57735-y

Tian, F., Herzschuh, U., Dallmeyer, A., Xu, Q., Mischke, S., & Biskaborn, B. K. (2013). Environmental variability in the monsoon-westerlies transition zone during the last 1200 years: Lake sediment analyses from central Mongolia and supra-regional synthesis. *Quaternary Science Reviews*, *73*, 31–47. https://doi.org/10.1016/j.quascirev.2013.05.005

Toney, J. L., García-Alix, A., Jiménez-Moreno, G., Anderson, R. S., Moossen, H., & Seki, O. (2020). New insights into Holocene hydrology and temperature from lipid biomarkers in western Mediterranean alpine wetlands. *Quaternary Science Reviews*, *240*, 106395. https://doi.org/10.1016/j.quascirev.2020.106395

Unkelbach, J., Kashima, K., Enters, D., Dulamsuren, C., Punsalpaamuu, G., & Behling, H. (2019). Late Holocene (Meghalayan) palaeoenvironmental evolution inferred from multi-proxy-studies of lacustrine sediments from the Dayan Nuur region of Mongolia. *Palaeogeography, Palaeoclimatology, Palaeoecology*, *530*, 1–14. https://doi.org/10.1016/j.palaeo.2019.05.021

Visbeck, M. (2002). Climate. The ocean's role in Atlantic climate variability. *Science*, *297*(5590), 2223–2224. https://doi.org/10.1126/science.1074029

Walther, M., Dashtseren, A., Kamp, U., Temujin, K., Meixner, F., Pan, C. G., et al. (2017). Glaciers, permafrost and lake levels at the Tsengel Khairkhan Massif, Mongolian Altai, during the late Pleistocene and Holocene. *Geosciences*, *7*(3), 73. https://doi.org/10.3390/geosciences7030073

Wang, W., & Feng, Z. (2013). Holocene moisture evolution across the Mongolian Plateau and its surrounding areas: A synthesis of climatic records. *Earth-Science Reviews*, *122*, 38–57. https://doi.org/10.1016/j.earscirev.2013.03.005

Willemse, N. W., & Törnqvist, T. E. (1999). Holocene century-scale temperature variability from West Greenland lake records. *Geology*, *27*(7), 580. https://doi.org/10.1130/0091-7613(1999)027<0580:hcstvf>2.3.co;2

Wolff, C., Plessen, B., Dudashvilli, A. S., Breitenbach, S. F. M., Cheng, H., Edwards, L. R., et al. (2017). Precipitation evolution of Central Asia during the last 5000 years. *The Holocene*, *27*(1), 142–154. https://doi.org/10.1177/0959683616652711

Yang, Y., Ran, M., & Sun, A. (2020). Pollen-recorded bioclimatic variations of the last ~2000 years retrieved from Bayan Nuur in the western Mongolian Plateau. *Boreas*, *49*(2), 350–362. https://doi.org/10.1111/bor.12423

References From the Supporting Information

Bliedtner, M., von Suchodoletz, H., Schäfer, I., Welte, I., Salazar, G., Szidat, S., et al. (2020). Age and origin of leaf wax n-alkanes in fluvial sediment-paleosol sequences and implications for paleoenvironmental reconstructions. *Hydrology and Earth System Sciences*, *24*(4), 2105–2120. https://doi.org/10.5194/hess-24-2105-2020

Douglas, P., Pagani, M., Eglinton, T., Brenner, M., Curtis, J., Breckenridge, A., et al. (2018). A long-term decrease in the persistence of soil carbon caused by ancient Maya land use. *Nature Geoscience*, *5*, 81. https://doi.org/10.1038/s41561-018-0192-7

Gierga, M., Hajdasvan Raden, I. U., Gilli, A., Wacker, L., Sturm, M., Sturm, M., et al. (2016). Long-stored soil carbon released by prehistoric land use. Evidence from compound-specific radiocarbon analysis on Soppensee lake sediments. *Quaternary Science Reviews*, *144*, 123–131. https://doi.org/10.1016/j.quascirev.2016.05.011

Hua, Q., Barbetti, M., & Rakowski, A. Z. (2013). Atmospheric radiocarbon for the period 1950–2010. *Radiocarbon*, *55*(4), 2059–2072. https://doi.org/10.2458/azu_js_rc.v55i2.16177

Lamb, A., Wilson, G., & Leng, M. (2006). A review of coastal palaeoclimate and relative sea-level reconstructions using $\delta^{13}C$ and C/N ratios in organic material. *Earth-Science Reviews*, *75*(1–4), 29–57. https://doi.org/10.1016/j.earscirev.2005.10.003

Meyers, P. A. (2003). Applications of organic geochemistry to paleolimnological reconstructions: A summary of examples from the Laurentian Great Lakes. *Organic Geochemistry*, *34*(2), 261–289. https://doi.org/10.1016/s0146-6380(02)00168-7

Ohlendorf, C., & Sturm, M. (2008). A modified method for biogenic silica determination. *Journal of Paleolimnology*, *39*(1), 137–142. https://doi.org/10.1007/s10933-007-9100-7

Reimer, P. J., Austin, W. E. N., Bard, E., Bayliss, A., Blackwell, P. G., Bronk Ramsey, C., et al. (2020). The IntCal20 Northern hemisphere radiocarbon age calibration curve (0–55 cal kBP). *Radiocarbon*, *62*(4), 725–757. https://doi.org/10.1017/RDC.2020.41

Ruff, M., Fahrni, S., Gaggeler, H. W., Hajdas, I., Suter, M., Synal, H.-A., et al. (2010). On-line Radiocarbon Measurements of small samples using elemental analyzer and MICADAS gas ion source. *Radiocarbon*, *52*, 1645–1656. https://doi.org/10.1017/s003382220005637x

Salazar, G., Zhang, Y. L., Agrios, K., & Szidat, S. (2015). Development of a method for fast and automatic radiocarbon measurement of aerosol samples by online coupling of an elemental analyzer with a MICADAS AMS. *Nuclear Instruments and Methods in Physics Research Section B: Beam Interactions With Materials and Atoms*, *361*, 163–167. https://doi.org/10.1016/j.nimb.2015.03.051

Wacker, L., Bonani, G., Friedrich, M., Hajdas, I., Kromer, B., Němec, M., et al. (2010). MICADAS: Routine and high-precision radiocarbon dating. *Radiocarbon*, *52*(02), 252–262. https://doi.org/10.1017/S0033822200045288